SUPPORTING INFORMATION FOR

Syntheses, Rearrangements, and Structural Analyses of Unsaturated Nitrogen Donor Ligands Derived from Diphenyldiazomethane and the Chiral Rhenium Lewis Acid $[(\eta^5\text{-}C_5H_5)Re(NO)(PPh_3)]^+$

Alexander L. Estrada,[a,‡] Taveechai Wititsuwannakul,[a,‡] Klemenz Kromm,[b] Frank Hampel,[b] Michael B. Hall,*[a] and John A. Gladysz*[a,b]

[a]Department of Chemistry, Texas A&M University, PO Box 30012, College Station, Texas 77843-3012, USA. E-mail: gladysz@mail.chem.tamu.edu

[b]Institut für Organische Chemie and Interdisciplinary Center for Molecular Materials, Friedrich-Alexander-Universität Erlangen-Nürnberg, Henkestraße 42, 91054 Erlangen, Germany

‡These authors contributed equally to this work.

S1. Computational details (continued)

Additional calculations were conducted with the CAM-B3LYP,[s1] M06,[s2] and BP86[s3] functionals to verify the results derived from the ωB97X-D functional. The calculations were performed at the level of CAM-B3LYP/BS2(CPCM)//CAM-B3LYP/BS1, M06/BS2(CPCM)//M06/BS1, or BP86/BS2(CPCM)//BP86/BS1 with solvation corrections for C_6H_5Cl with UFF atomic radii in combination with the "Dis", "Rep", and "Cav" keywords.

Furthermore, for *sc*-**5**$^+$ and *ac*-**5**$^+$, dispersion corrections were implemented using the D3 version of Grimme's dispersion function with Becke-Johnson damping (referred to as GD3BJ)[s4] at the level of CAM-BLYP-GD3BJ/BS1, BP86-GD3BJ/BS1, CAM-B3LYP-GD3BJ/BS2(C-PCM)//CAM-B3LYP-GD3BJ/BS1, or BP86-GD3BJ/BS2(CPCM)//BP86-GD3BJ/BS1 with solvation corrections as described above.

S2. Structures of and bonding in rhenium complexes

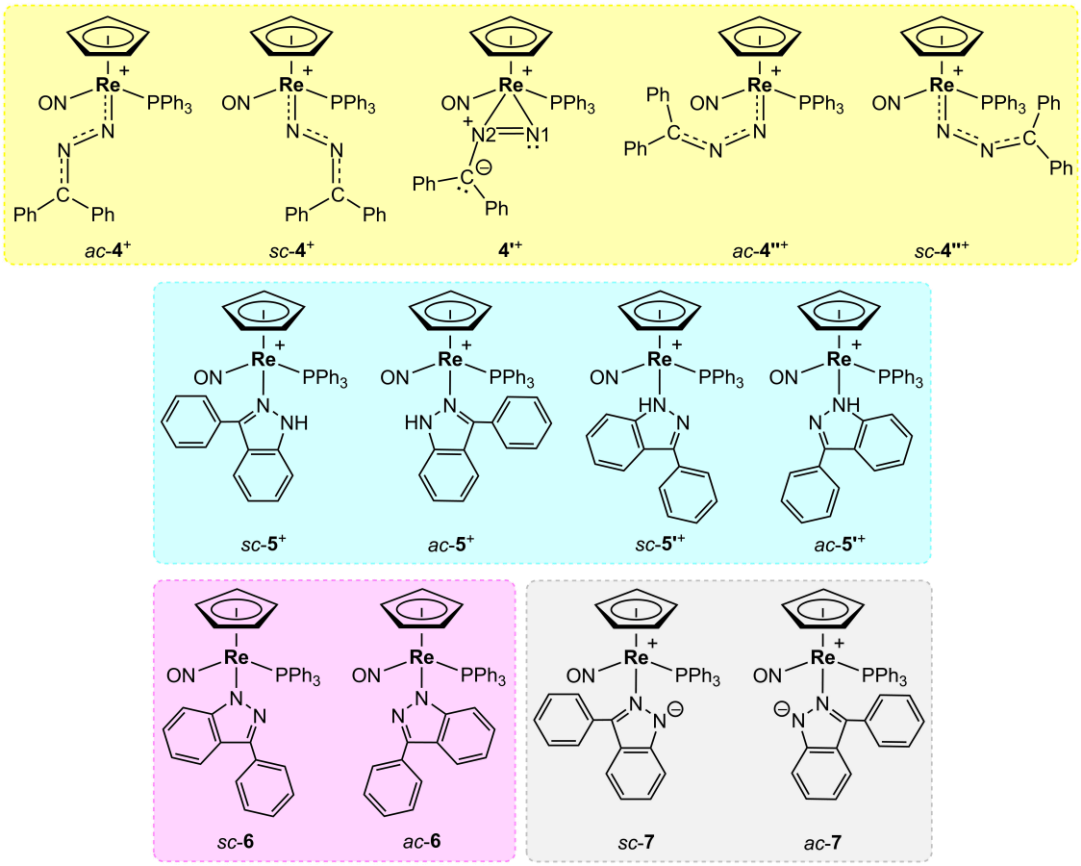

Figure S1. Representations of rhenium complexes investigated computationally. Minima for *ac*-**4″**$^+$ and *sc*-**4″**$^+$ could not be located.

Table S1. Re-NN bond lengths (Å) of the gas-phase optimized structures of the complexes in Figure S1 using four different DFT functionals.

complex	experimental data	ωB97X-D/BS1[a]	CAM-B3LYP/BS1[a]	M06/BS1[a]	BP86/BS1[a]
ac-**4**$^+$	1.914(3)	1.925	1.930	1.916	1.876
sc-**4**$^+$	-	1.964	1.967	1.956	1.909
4′$^+$	-	2.066[b]	2.062[b]	2.063[b]	2.084[b]
		2.017[c]	2.028[c]	2.027[c]	2.047[c]
sc-**5**$^+$	2.137(6)	2.131	2.134	2.143	2.124
ac-**5**$^+$	-	2.152	2.156	2.164	2.153
sc-**5′**$^+$	-	2.240	2.239	2.257	2.257
ac-**5′**$^+$	-	2.253	2.258	2.274	2.275
sc-**6**	2.095(5)	2.072	2.070	2.072	2.075
ac-**6**	-	2.098	2.099	2.111	2.099
sc-**7**	-	2.102	2.100	2.108	2.100
ac-**7**	-	2.120	2.122	2.130	2.119

[a]BS1 = LANL2DZ+f for the rhenium atom and 6-31G(d,p) for other atoms. [b]Re-N1 (see Figure S2). [c]Re-N2 (see Figure S2).

Table S2. N-N bond lengths (Å) of the gas-phase optimized structures of the complexes in Figure S1 using four different DFT functionals.

complex	experimental data	ωB97X-D/BS1[a]	CAM-B3LYP/BS1[a]	M06/BS1[a]	BP86/BS1[a]
ac-**4**$^+$	1.206(4)	1.198	1.194	1.207	1.234
sc-**4**$^+$	-	1.191	1.179	1.196	1.219
4′$^+$	-	1.264	1.265	1.270	1.286
sc-**5**$^+$	1.342(8)	1.360	1.363	1.364	1.384
ac-**5**$^+$	-	1.364	1.366	1.368	1.384
sc-**5′**$^+$	-	1.433	1.440	1.435	1.463
ac-**5′**$^+$	-	1.438	1.442	1.437	1.463
sc-**6**	1.379(7)	1.352	1.355	1.354	1.371
ac-**6**	-	1.353	1.354	1.354	1.370
sc-**7**	-	1.351	1.352	1.353	1.370
ac-**7**	-	1.354	1.354	1.355	1.374

[a]BS1 = LANL2DZ+f for the rhenium atom and 6-31G(d,p) for other atoms.

Table S3. Angles (°) between the C_7N_2 and C_6 least square planes, and distances (Å) between the centroids of the five- and six-membered rings (C_6(phenyl), C_3N_2, C_6(benzenoid)) of the diphenyldiazomethane, indazole, or indazolyl ligand and that of the proximal PPh_3 phenyl ring (C_6H_5), and any NH/π or CH/π interactions.[a,b] Experimental values are given in brackets [] when available.

complex	C_7N_2 and C_6 least square planes	C_6(phenyl)···C_6H_5 centroids	C_3N_2···C_6H_5 centroids	C_6(benzenoid)···C_6H_5 centroids	N···(C_6H_5 centroid)	H_N···(C_6H_5 centroid)[c]	H(phenyl)···(C_6H_5 centroid)	H(C_6H_5)···(C_6(phenyl) centroid)
ac-**4**$^+$[d]	-	3.761 [4.056]	-	-	4.203,[e] 3.768[f] [4.141,[e] 3.715][f]	-	-	-
sc-**4**$^+$[g]	-	-	-	-	4.007,[e] 4.167[f]	-	2.624[h]	-
4′$^+$[i]	-	-	-	-	3.820,[e] 4.794[f]	-	-	-
sc-**5**$^+$[j]	36.65 [23.70]	-	3.954 [3.731]	4.596 [4.362]	4.054,[e] 4.007[f] [3.879,[e] 3.613][f]	4.263[k] [3.761][l]	-	-
ac-**5**$^+$	35.12	-	4.207	5.053	4.152,[e] 4.678[f]	5.234[m]	2.558[n]	2.331[o]
sc-**5′**$^+$[p]	8.38	-	3.885	3.686	4.512,[e] 4.476[f]	-	-	3.270[q]
ac-**5′**$^+$[r]	8.96	-	3.787	3.860	4.288,[e] 4.392[f]	-	-	-
sc-**6**	33.20 [42.29]	-	3.841 [4.012]	5.048 [5.250]	3.892,[e] 3.559[f] [3.969,[e] 3.671][f]	-	3.145[s] [3.276][t]	-
ac-**6**	38.49	-	3.880	4.223	4.001,[e] 4.199[f]	-	-	-

(continued)

Table S3 continued

complex	C_7N_2 and C_6 least square planes	C_6(phenyl)···C_6H_5 centroids	C_3N_2···C_6H_5 centroids	C_6(benzenoid)···C_6H_5 centroids	N···(C_6H_5 centroid)	H_N···(C_6H_5 centroid)[c]	H(phenyl)···(C_6H_5 centroid)	H(C_6H_5)···(C_6(phenyl) centroid)
sc-**7**[u]	16.39	-	3.452	3.793	3.753,[e] 3.603[f]	-	-	-
ac-**7**	36.46	-	4.178	4.963	4.162,[e] 4.684[f]	-	2.564[v]	2.289[w]

[a]See Figures S2-S6. [b]All values derived from optimized geometries at the level of ωB97X-D/BS1 (BS1 = LANL2DZ+f for the rhenium atom and 6-31G(d,p) for non-metal atoms). [c]Distance N_2H_1···(C_6H_5 centroid). [d]Additional angle of the least squares planes of the diphenyldiazomethane and PPh_3 phenyl groups: 5.04° [20.75°]. [e]Distance N_1···(C_6H_5 centroid). [f]Distance N_2···(C_6H_5 centroid). [g]Additional distance/angle (C_6(phenyl) centroid)···H-C(C_5H_5): 2.712 Å/149.65°. [h]Angle C-H···(C_6H_5 centroid): 155.51°. [i]Additional distance/angle (C_6(phenyl) centroid)···H-C(C_5H_5): 2.642 Å/132.22°. [j]Additional distance (C_6(benzenoid) centroid)···O: 3.386 [3.258] Å. [k]Angle N_2-H_1···(C_6H_5 centroid): 68.59°. [l]Angle N_2-H_1···(C_6H_5 centroid): 73.63°. [m]Angle N_2-H_1···(C_6H_5 centroid): 51.70°. [n]Angle C-H···(C_6H_5 centroid): 127.75°. [o]Angle C-H···(C_6(phenyl) centroid): 164.44°. [p]Additional distance/angle (C_3N_2 centroid)···H-C(C_6H_5): 3.169 Å/146.33°. [q]Angle C-H···(C_6(phenyl) centroid): 133.92°. [r]Additional distance/angle (C_6(benzenoid) centroid)···H-C(C_6H_5): 3.197 Å/164.91°. [s]Angle C-H···(C_6H_5 centroid): 128.82°. [t]Angle C-H···(C_6H_5 centroid): 139.66°. [u]Additional distance (C_6(benzenoid) centroid)···O: 3.501 Å. [v]Angle C-H···(C_6H_5 centroid): 127.79°. [w]Angle C-H···(C_6(phenyl) centroid): 163.43°.

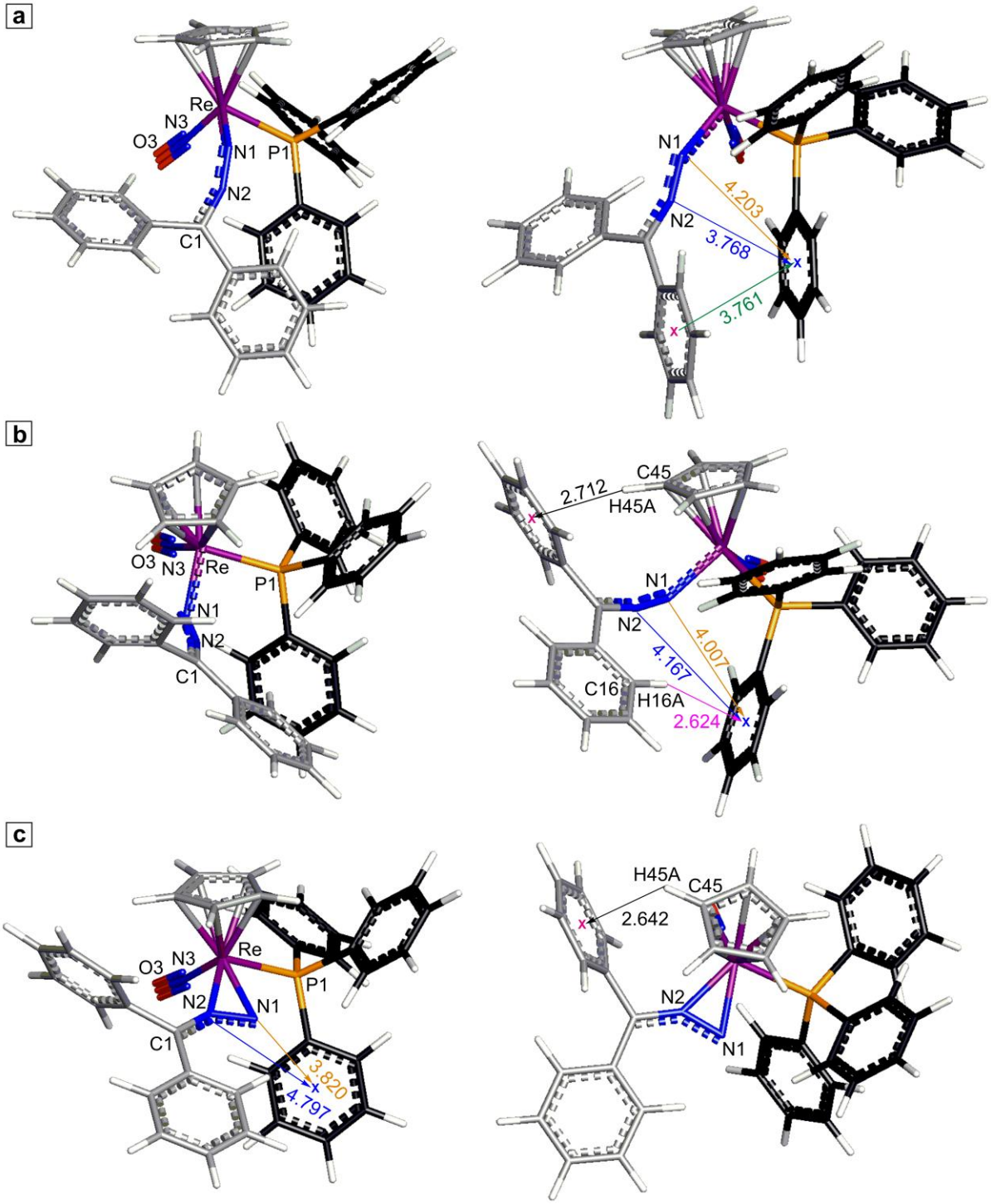

Figure S2. Optimized geometries of (a) *ac*-**4**$^{+}$, (b) *sc*-**4**$^{+}$, and (c) **4′**$^{+}$. The distances (Å) between the centroids associated with a phenyl ring (C_6(phenyl)) of the diphenyldiazomethane ligand and the proximal PPh_3 phenyl ring, and the nitrogen atoms (N1 and N2) of the diphenyldiazomethane ligand and the centroid of the proximal PPh_3 phenyl ring, are shown in green, orange, and blue, respectively. The distances from a hydrogen atom (H45A) of the cyclopentadienyl ligand to the centroid of a phenyl ring of the diphenyldiazomethane ligand and from the hydrogen atom (H16A) of the phenyl ring of the diphenyldiazomethane ligand to the centroid of the proximal PPh_3 phenyl ring are shown in black and magenta, respectively. The C45-H45A···(C_6(phenyl) centroid) angles of *sc*-**4**$^{+}$ and **4′**$^{+}$ and the C16-H16A···(C_6H_5 centroid) angle of *sc*-**4**$^{+}$ are 149.65°, 132.22°, and 155.51°, respectively.

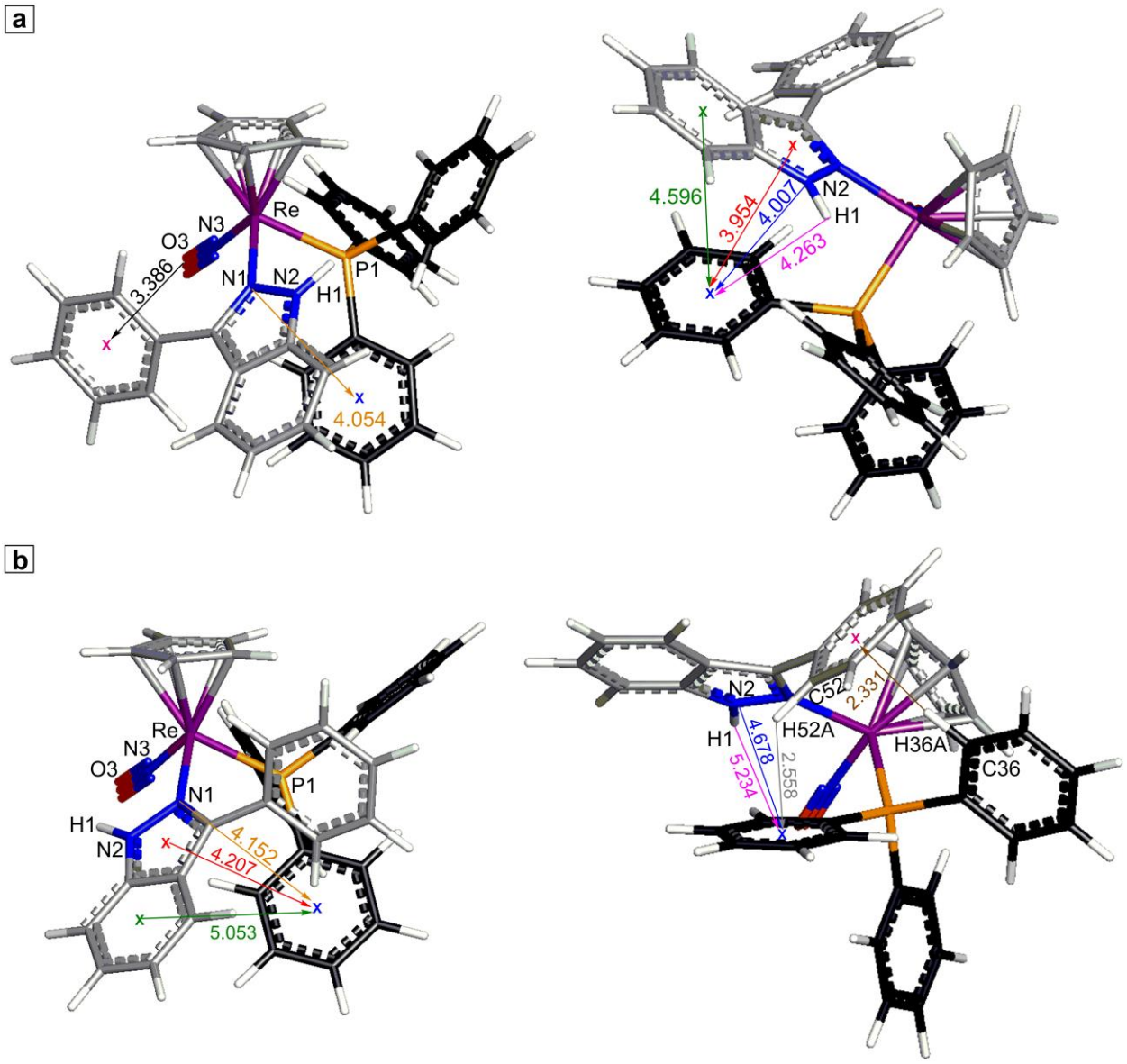

Figure S3. Optimized geometries of (a) *sc*-**5**$^{+}$ and (b) *ac*-**5**$^{+}$. The distances (Å) between the centroids associated with five- and six-membered indazole rings (C_3N_2 and C_6(benzenoid)) and the proximal PPh_3 phenyl ring, and from the nitrogen (N1 and N2) and hydrogen (H1) atoms of the indazole ring to the centroid of the proximal PPh_3 phenyl ring, are shown in red, green, orange, blue, and magenta, respectively. The distance from the oxygen atom (O3) to the centroid of the indazole phenyl ring is shown in black. The distances from the hydrogen (H52A) atom of the indazole phenyl ring to the centroid of the proximal PPh_3 phenyl ring and from the hydrogen atom (H36A) of the proximal PPh_3 phenyl ring to the centroid of the indazole phenyl ring are shown in gray and brown, respectively. The C52-H52A···(C_6H_5 centroid) and C36-H36A···(C_6(phenyl) centroid) angles are 127.75° and 164.44°, respectively.

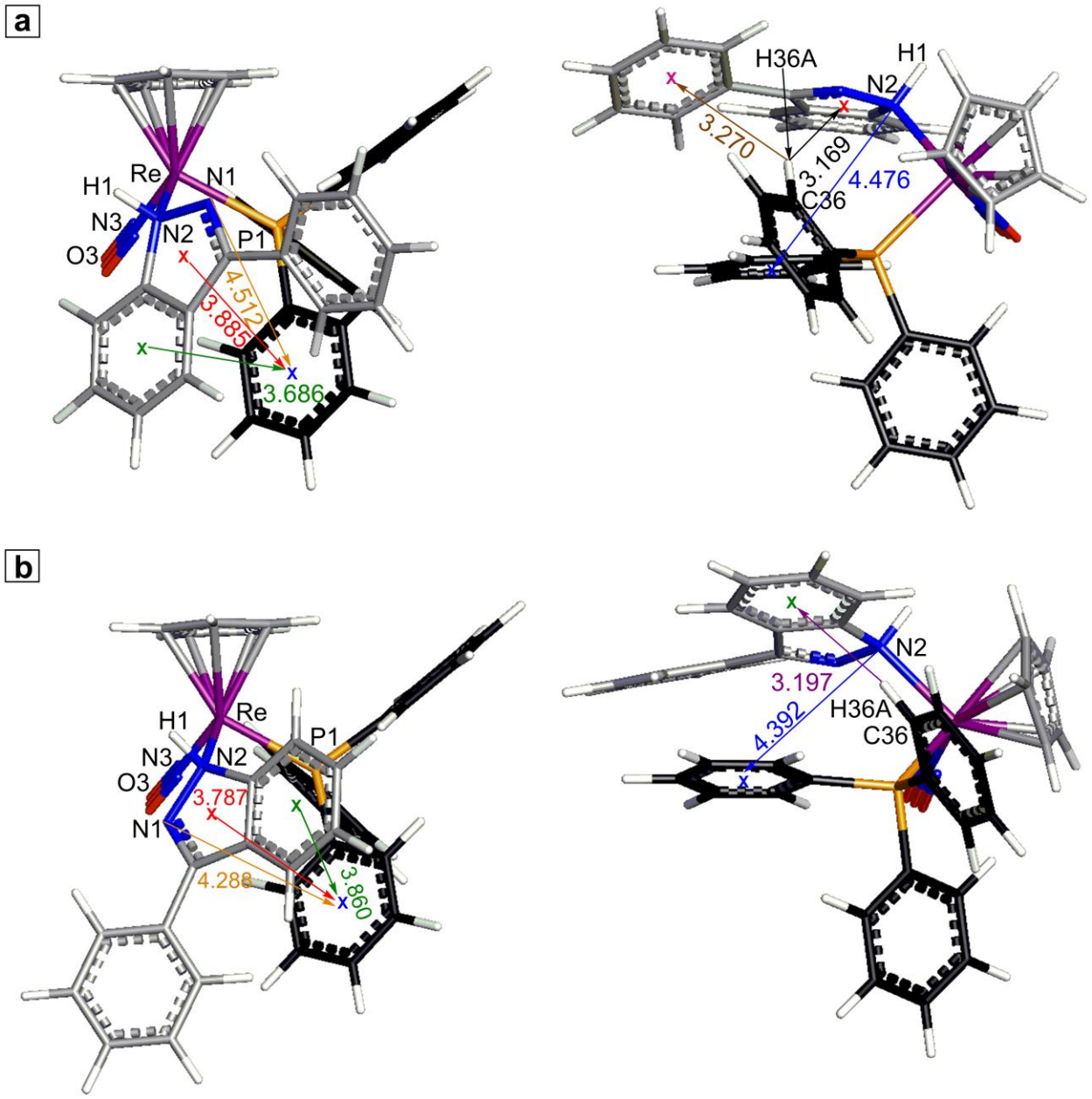

Figure S4. Optimized geometries of (a) *sc*-**5′**$^{+}$ and (b) *ac*-**5′**$^{+}$. The distances (Å) between the centroids associated with five- and six-membered indazole rings (C_3N_2 and C_6(benzenoid)) and the proximal PPh_3 phenyl ring, and from the nitrogen atoms (N1 and N2) of the indazole ring to the centroid of the proximal PPh_3 phenyl ring, are shown in red, green, orange, and blue, respectively. The distances from the hydrogen (H36A) atom of the proximal PPh_3 phenyl ring to the centroids of five- and six-membered indazole rings and the indazole phenyl ring are shown in black, purple, and brown, respectively. The C36-H36A···(C_3N_2 centroid), C36-H36A···(C_6(benzenoid) centroid), and C36-H36A···(C_6(phenyl) centroid) angles are 146.33°, 164.91°, and 133.92°, respectively.

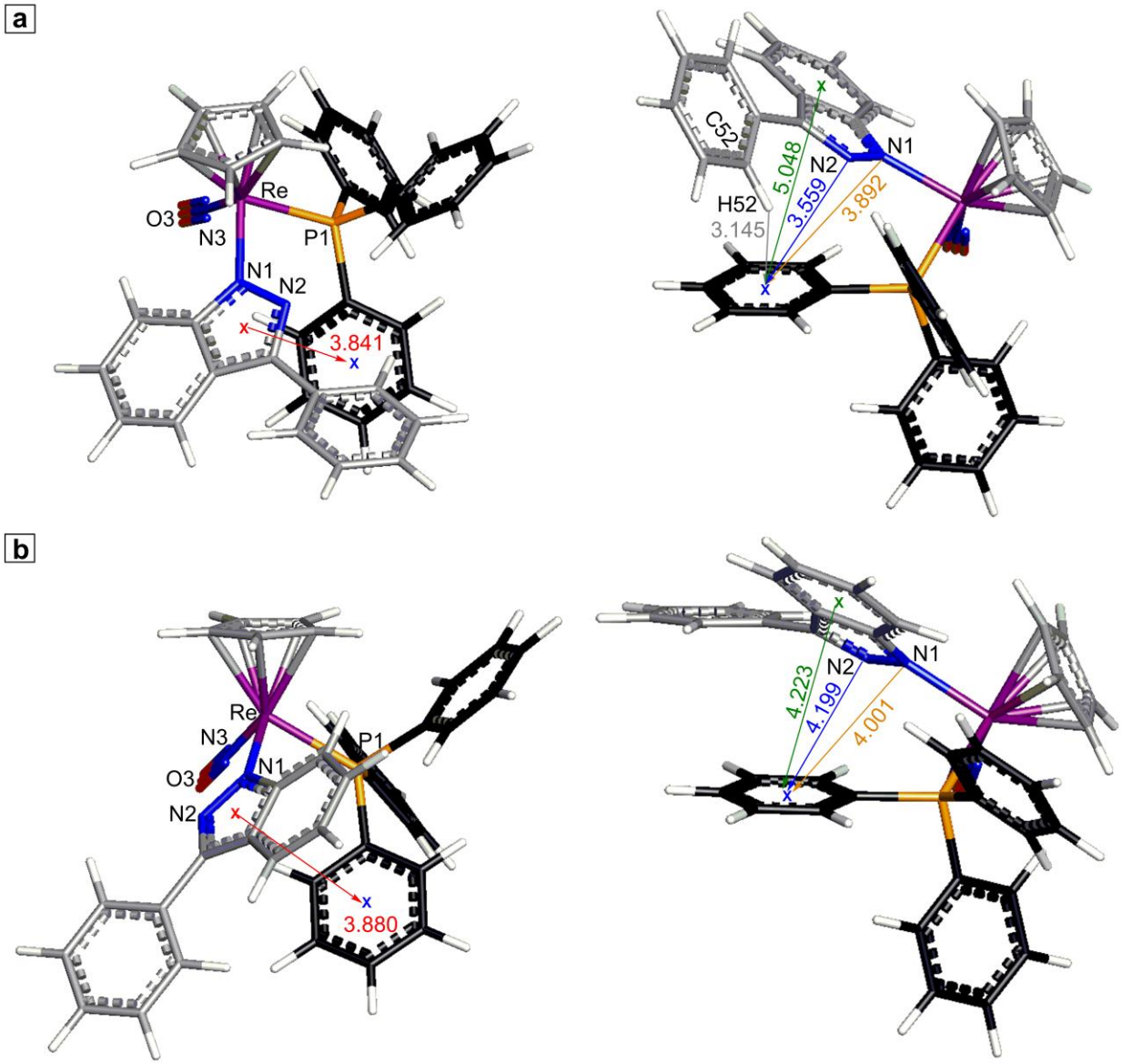

Figure S5. Optimized geometries of (a) *sc*-**6** and (b) *ac*-**6**. The distances (Å) between the centroids associated with five- and six-membered indazolyl rings (C_3N_2 and C_6(benzenoid)) and the proximal PPh_3 phenyl ring, and the nitrogen (N1 and N2) and hydrogen (H1) atoms of the indazolyl ring and the centroid of the proximal PPh_3 phenyl ring, are shown in red, green, orange, and blue, respectively. The distance from the hydrogen (H52) atom of the phenyl ring of the indazolyl ligand to the centroid of the proximal PPh_3 phenyl ring is shown in gray. The C52-H52···(C_6H_5 centroid) angle is 128.82°.

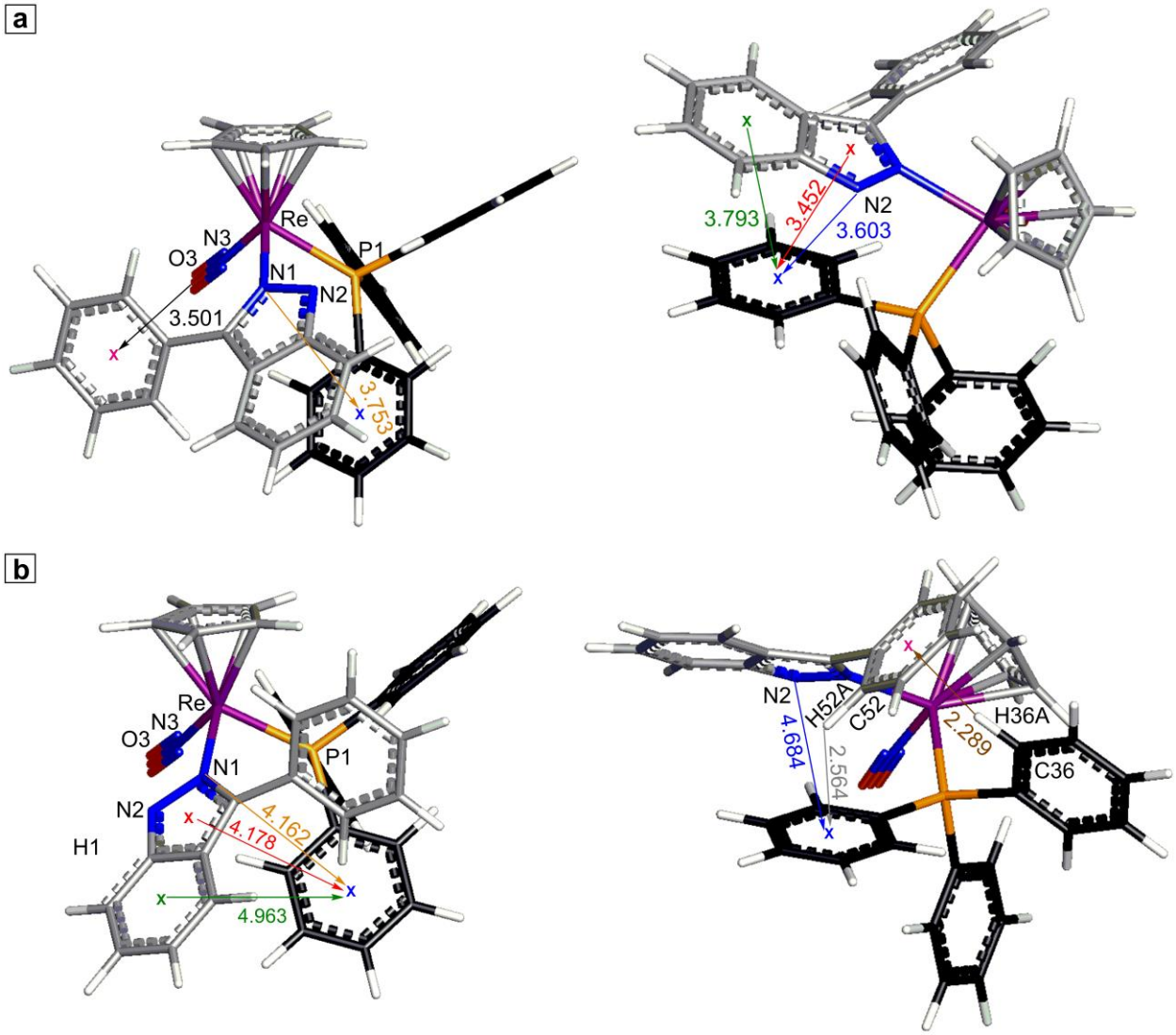

Figure S6. Optimized geometries of (a) *sc*-**7** and (b) *ac*-**7**. The distances (Å) between the centroids associated with five- and six-membered indazolyl rings (C_3N_2 and C_6(benzenoid)) and the proximal PPh_3 phenyl ring, and from the nitrogen (N1 and N2) atoms of the indazolyl ring to the centroid of the proximal PPh_3 phenyl ring, are shown in red, green, orange, and blue, respectively. The distance from the oxygen atom (O3) to the centroid of the indazolyl phenyl ring is shown in black. The distances from the hydrogen (H52A) atom of the indazolyl phenyl ring to the centroid of the proximal PPh_3 phenyl ring and from the hydrogen atom (H36A) of the proximal PPh_3 phenyl ring to the centroid of the indazolyl phenyl ring are shown in gray and brown, respectively. The C52-H52A···(C_6H_5 centroid) and C36-H36A···(C_6(phenyl) centroid) angles are 127.79° and 163.43°, respectively.

Table S4. Relative gas-phase free energies (ΔG(gas), kcal/mol) for the species in Figure S1 using four different DFT functionals.[a]

complex	ωB97X-D/BS1[b]	CAM-B3LYP/BS1[b]	M06/BS1[b]	BP86/BS1[b]
ac-**4**$^+$	0.0	0.0	0.0	0.0
sc-**4**$^+$	2.8	2.8	3.2	2.1
4′$^+$	16.3	19.1	16.9	17.8
sc-**5**$^+$	0.0	0.0[c]	0.0	0.0[d]
ac-**5**$^+$	–1.0	4.4[c]	–2.8	4.3[d]
sc-**5′**$^+$	14.9	20.5	14.2	21.1
ac-**5′**$^+$	22.0	25.8	19.0	26.0
sc-**6**	0.0	0.0	0.0	0.0
ac-**6**	8.9	8.8	8.1	7.2
sc-**7**	0.0	0.0	0.0	0.0
ac-**7**	6.7	9.2	6.3	9.1

[a]See also Table S7. [b]BS1 = LANL2DZ+f for the rhenium atom and 6-31G(d,p) for non-metal atoms. [c]The gas-phase free energy of *sc*-**5**$^+$ derived from the level of CAM-B3LYP-GD3BJ/BS1 is lower than that of *ac*-**5**$^+$ by –1.4 kcal/mol, compared to –4.4 kcal/mol (without the GD3BJ dispersion corrections) derived from the level of CAM-B3LYP/BS1. [d]The gas-phase free energy of *sc*-**5**$^+$ derived from the level of BP86-GD3BJ/BS1 is higher than that of *ac*-**5**$^+$ by 0.6 kcal/mol, compared to lower by –4.3 kcal/mol (without the GD3BJ dispersion corrections) derived from the level of BP86/BS1. This indicates that steric interactions (including dispersion) render *ac*-**5**$^+$ slightly more stable than *sc*-**5**$^+$. This conclusion is consistent with the results of other functionals in this table.

Table S5. Relative free energies in C_6H_5Cl solution ($\Delta G(C_6H_5Cl)$, kcal/mol) for the species in Figure S1 using four different DFT functionals.[a]

complex	$\Delta G(C_6H_5Cl)$			
	ωB97X-D[b]	CAM-B3LYP[c]	M06[d]	BP86[e]
ac-**4**$^+$	0.0	0.0	0.0	0.0
sc-**4**$^+$	2.4	1.5	2.3	0.3
4′$^+$	11.1	13.4	12.7	13.1
sc-**5**$^+$	0.0	0.0[f]	0.0	0.0[g]
ac-**5**$^+$	–1.2	2.0[f]	–3.4	4.3[g]
sc-**5′**$^+$	16.2	19.6	15.6	22.2
ac-**5′**$^+$	21.0	22.6	18.5	24.6
sc-**6**	0.0	0.0	0.0	0.0
ac-**6**	5.3	5.5	4.2	3.8
sc-**7**	0.0	0.0	0.0	0.0
ac-**7**	3.2	6.4	2.7	7.0

[a]See also Table S7. [b]Single point calculations at the level of ωB97X-D/BS2(CPCM)//ωB97X-D/BS1 with solvation corrections for C_6H_5Cl with UFF atomic radii (BS1 = LANL2DZ+f for the rhenium atom and 6-31G(d,p) for non-metal atoms and BS2 = LANL2TZ(f) for the rhenium atom and def2-TZVP for non-metal atoms). [c]Single point calculations at the level of CAM-B3LYP/BS2(CPCM)//CAM-B3LYP/BS1 with solvation corrections for C_6H_5Cl with UFF atomic radii. [d]Single point calculations at the level of M06/BS2(CPCM)//M06/BS1 with solvation corrections for C_6H_5Cl with UFF atomic radii. [e]Single point calculations at the level of BP86/BS2(CPCM)//BP86/BS1 with solvation corrections for C_6H_5Cl with UFF atomic radii. [f]With the GD3BJ dispersion corrections, the solution-phase free energy derived from the level of CAM-B3LYP-GD3BJ/BS2(CPCM)//CAM-B3LYP-GD3BJ/BS1 with solvation corrections for C_6H_5Cl with UFF atomic radii for *sc*-**5**$^+$ is higher than that for *ac*-**5**$^+$ by 1.6 kcal/mol, compared to lower by –2.0 kcal/mol (without the GD3BJ dispersion corrections) derived from the level of CAM-B3LYP/BS2(CPCM)//CAM-B3LYP/BS1 with solvation corrections for C_6H_5Cl with UFF atomic radii. [g]With the GD3BJ dispersion corrections, the solution-phase free energy derived from the level of BP86-GD3BJ/BS2(CPCM)//BP86-GD3BJ/BS1 with solvation corrections for C_6H_5Cl with UFF atomic radii for *sc*-**5**$^+$ is higher than that for *ac*-**5**$^+$ by 2.7 kcal/mol, compared to lower by –4.3 kcal/mol (without the GD3BJ dispersion corrections) derived from the level of BP86/BS2(CPCM)//BP86/BS1 with solvation corrections for C_6H_5Cl with UFF atomic radii. This indicates that steric interactions (including dispersion) render *ac*-**5**$^+$ slightly more stable than *sc*-**5**$^+$. This conclusion is consistent with the results of other functionals in this table.

Table S6. Selected Wiberg bond indices for the complexes in Figures S1 and the corresponding computed bond lengths (Å) of the gas-phase optimized structures.[a,b,c] When available, experimental values are given in brackets [].

complex	Wiberg bond index			bond length		
	Re-NN	N-N	N-C(Ph_2)	Re-NN	N-N	N-C(Ph_2)
ac-**4**$^+$	0.83	1.79	1.55	1.925 [1.914(3)]	1.198 [1.206(4)]	1.277 [1.292(4)]
sc-**4**$^+$	0.76	1.85	1.54	1.964	1.191	1.277
4′$^+$	0.71[d] 0.50[e]	1.44	1.43	2.066[d] 2.017[e]	1.264	1.305
sc-**5**$^+$	0.42	1.12	-	2.131 [2.137(6)]	1.360 [1.342(8)]	-
ac-**5**$^+$	0.41	1.13	-	2.152	1.364	-
sc-**5′**$^+$	0.33	1.02	-	2.240	1.433	-
ac-**5′**$^+$	0.32	1.02	-	2.253	1.438	-
sc-**6**	0.51	1.22	-	2.072 [2.095(5)]	1.352 [1.379(7)]	-
ac-**6**	0.49	1.23	-	2.098	1.353	-
sc-**7**	0.48	1.24	-	2.102	1.351	-
ac-**7**	0.47	1.26	-	2.120	1.354	-

[a]Optimization at the level of ωB97X-D/BS1 (BS1 = LANL2DZ+f for the rhenium atom and 6-31G(d,p) for non-metal atoms). [b]The Wiberg bond indices correlate well with the bond lengths. [c]The computed N-N bond length of dinitrogen (N_2) is 1.102 Å, and the Wiberg bond index (3.02) is very close to the formal bond order (3). [d]Re-N1 (see Figure S2). [e]Re-N2 (see Figure S2).

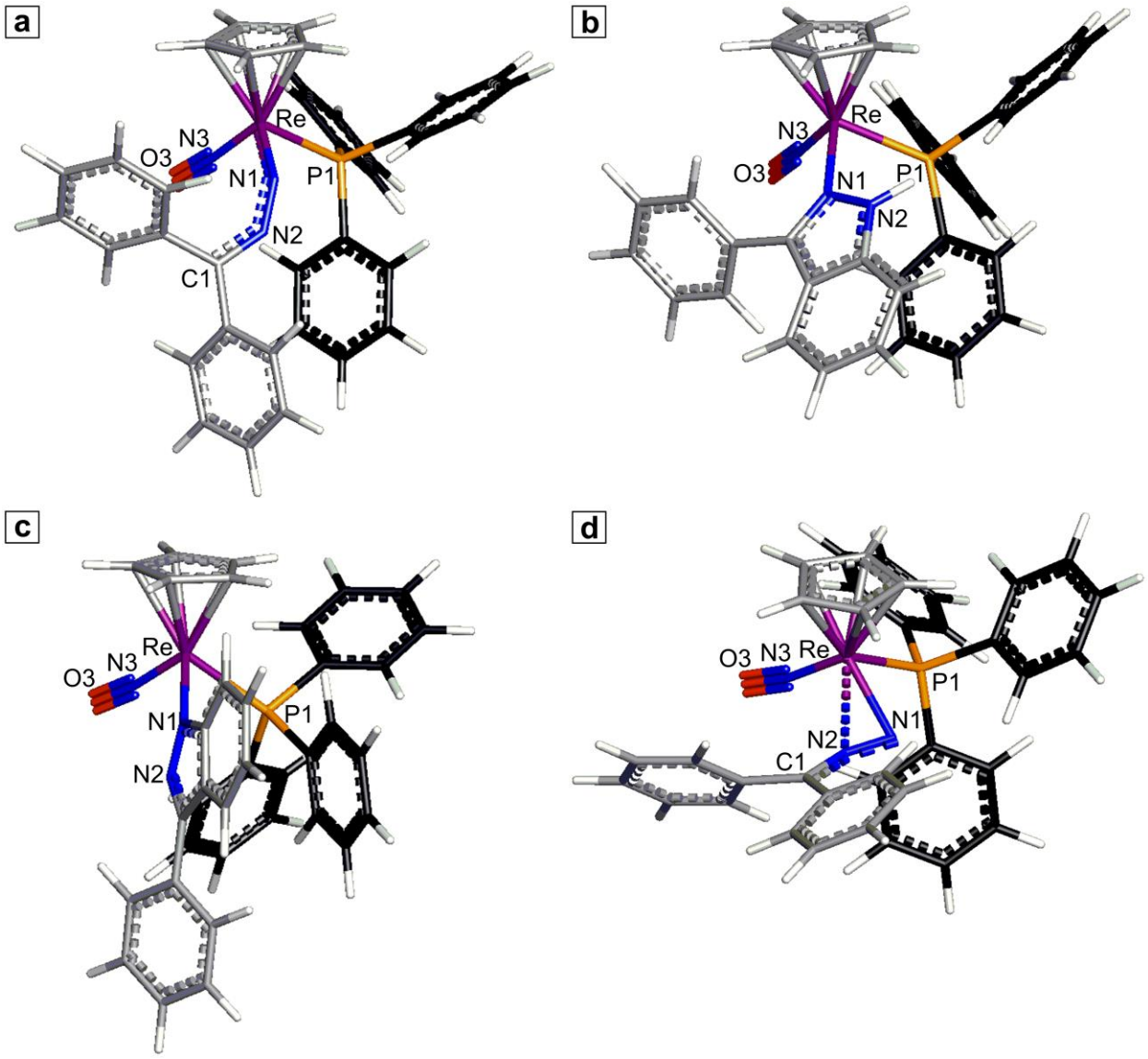

Figure S7. Optimized geometries of (a) $\mathbf{TS_{rot}a}$ (the transition state for interconverting *ac*-$\mathbf{4}^+$ and *sc*-$\mathbf{4}^+$), (b) $\mathbf{TS_{rot}b}$ (the transition state for interconverting *sc*-$\mathbf{5}^+$ and *ac*-$\mathbf{5}^+$), (c) $\mathbf{TS_{rot}c}$ (the transition state for interconverting *sc*-**6** and *ac*-**6**), and (d) $\mathbf{TS_{ReN}d}$ (the transition state for interconverting *ac*-$\mathbf{4}^+$ and $\mathbf{4'}^+$). Selected distances (Å), angles, and torsion angles (°): $\mathbf{TS_{rot}a}$, Re-N1 1.869, N1-N2 1.246, C1-N2-N1 136.00, N2-N1-Re 131.27, N2-N1-Re-N3 14.57, C1-N2-N1-Re –76.57; $\mathbf{TS_{rot}b}$, Re-N1 2.134, N1-N2 1.366, N2-N1-Re-N3 148.61; $\mathbf{TS_{rot}c}$, Re-N1 2.122, N1-N2 1.349, N2-N1-Re-N3 29.57; $\mathbf{TS_{ReN}d}$, Re-N1 2.165, Re-N2 2.415, N1-N2 1.198, Re-N1-N2 86.78, Re-N2-N1 63.52, N1-Re-N2 29.70. See Table S7 for the energies.

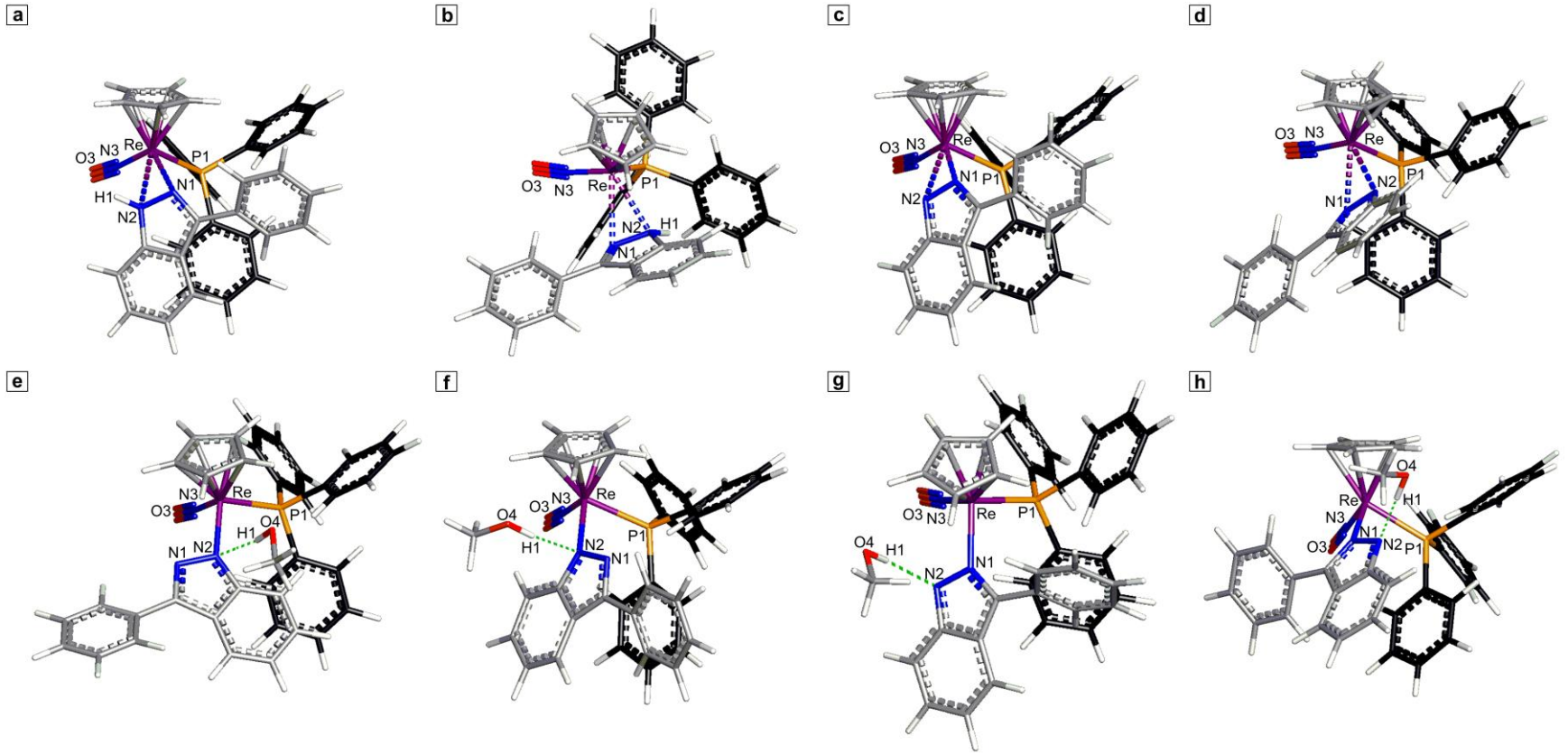

Figure S8. Optimized geometries of (a) $\mathbf{TS_{ReN}e}$ (the transition state for interconverting *ac*-**5**$^{+}$ and *sc*-**5′**$^{+}$), (b) $\mathbf{TS_{ReN}f}$ (the transition state for interconverting *sc*-**5**$^{+}$ and *ac*-**5′**$^{+}$), (c) $\mathbf{TS_{ReN}g}$ (the transition state for interconverting *ac*-**7** and *sc*-**6**), (d) $\mathbf{TS_{ReN}h}$ (the transition state for interconverting *sc*-**7** and *ac*-**6**), (e) *ac*-**5′**-OCH_3, (f) *sc*-**5′**-OCH_3, (g) *ac*-**5**-OCH_3, and (h) *sc*-**5**-OCH_3. Selected distances (Å) and N2-H1-O4 angles (°): $\mathbf{TS_{ReN}e}$, Re-N1 2.604, Re-N2 2.517, N1-N2 1.398; $\mathbf{TS_{ReN}f}$, Re-N1 2.587, Re-N2 2.524, N1-N2 1.398; $\mathbf{TS_{ReN}g}$, Re-N1 2.344, Re-N2 2.432, N1-N2 1.356; $\mathbf{TS_{ReN}h}$, Re-N1 2.436, Re-N2 2.313, N1-N2 1.361; *ac*-**5′**-OCH_3, Re-N2 2.097, N1-N2 1.361, N2-H1 2.380, O4-H1 0.965, N2-H1-O4 171.56; *sc*-**5′**-OCH_3, Re-N2 2.108, N1-N2 1.356, N2-H1 2.125, O4-H1 0.966, N2-H1-O4 165.45; *ac*-**5**-OCH_3, Re-N1 2.124, N1-N2 1.358, N2-H1 1.903, O4-H1 0.977, N2-H1-O4 153.49; *sc*-**5**-OCH_3, Re-N1 2.111, N1-N2 1.352, N2-H1 1.781, O4-H1 0.983, N2-H1-O4 173.85. See Table S7 for the energies.

S3. Miscellaneous

Table S7. Relative gas-phase electronic energies, enthalpies, entropies, free energies, and solution-phase free energies (C_6H_5Cl) with solvation corrections at 1.0 atm or 1.0 M (both 298.15 K) for the species in Figures S1, S7, S8, 8, and 9 (main text).

	ωB97X-D/BS1[a]				ωB97X-D/BS2(CPCM)// ωB97X-D/BS1[a,b]	
	ΔE(gas) (kcal/mol)	ΔH(gas) (kcal/mol)	ΔS(gas) (cal/K·mol)	ΔG(gas) (kcal/mol)	$\Delta G(C_6H_5Cl)$ (1.0 atm) (kcal/mol)	$\Delta G(C_6H_5Cl)$ (1.0 M) (kcal/mol)
ac-**4**$^+$	0.0	0.0	0.0	0.0	0.0	0.0
sc-**4**$^+$	3.4	3.4	1.9	2.8	2.4	2.4
TS$_{rot}$a[c]	5.0	4.4	–5.8	6.2	6.0	6.0
4′$^+$	15.2	15.4	–3.2	16.3	11.1	11.1
TS$_{ReN}$d[d]	30.3	29.2	1.6	28.7	27.1	27.1
sc-**5**$^+$	0.0	0.0	0.0	0.0	0.0	0.0
ac-**5**$^+$	–3.1	–2.9	–6.3	–1.0	–1.2	–1.2
TS$_{rot}$b[e]	0.4	–0.7	–4.9	0.8	1.5	1.5
sc-**5′**$^+$	14.0	13.9	–3.4	14.9	16.2	16.2
ac-**5′**$^+$	21.1	21.0	–3.3	22.0	21.0	21.0
sc-**6**	0.0	0.0	0.0	0.0	0.0	0.0
ac-**6**	7.8	8.0	–2.9	8.9	5.3	5.3
TS$_{rot}$c[f]	10.4	9.8	–10.8	13.1	10.9	10.9
ac-**5**$^+$ + $^-OCH_3$[g]	0.0	0.0	0.0	0.0	0.0	0.0
sc-**5**$^+$ + $^-OCH_3$[g]	3.1	2.9	6.3	1.0	1.2	1.2
TS$_{ReN}$e[h] + $^-OCH_3$[g]	25.7	24.5	–0.8	24.8	26.7	26.7
TS$_{ReN}$f[i] + $^-OCH_3$[g]	29.8	28.6	5.8	26.9	29.5	29.5
ac-**5′**$^+$ + $^-OCH_3$[j,g]	24.2	23.9	2.9	23.1	22.2	22.2
sc-**5′**$^+$ + $^-OCH_3$[k,g]	17.0	16.8	2.9	15.9	17.3	17.3
ac-**5′**-OCH_3[j,l]	–143.5	–140.1	–24.9	–132.7	–42.4	–44.3
sc-**5′**-OCH_3[k,m]	–153.9	–150.7	–29.5	–141.9	–49.6	–51.5
ac-**6** + CH_3OH[l,g]	–133.6	–131.8	6.8	–133.8	–50.1	–50.1
sc-**6** + CH_3OH[m,g]	–141.4	–139.8	9.7	–142.7	–55.4	–55.4
ac-**5**$^+$ + $^-OCH_3$[n,g]	0.0	0.0	0.0	0.0	0.0	0.0
sc-**5**$^+$ + $^-OCH_3$[o,g]	3.1	2.9	6.3	1.0	1.2	1.2
ac-**5**-OCH_3[n,p]	–150.1	–146.5	–34.6	–136.2	–46.0	–47.9
sc-**5**-OCH_3[o,q]	–153.9	–150.6	–29.9	–141.7	–50.0	–51.9

(continued)

Table S7 continued

	ωB97X-D/BS1[a]				ωB97X-D/BS2(CPCM)// ωB97X-D/BS1[a,b]	
	Δ*E*(gas) (kcal/mol)	Δ*H*(gas) (kcal/mol)	Δ*S*(gas) (cal/K·mol)	Δ*G*(gas) (kcal/mol)	Δ*G*(C_6H_5Cl) (1.0 atm) (kcal/mol)	Δ*G*(C_6H_5Cl) (1.0 M) (kcal/mol)
ac-**7** + CH_3OH[p,g]	–131.9	–130.0	0.7	–130.2	–47.4	–47.4
sc-**7** + CH_3OH[q,g]	–136.9	–135.2	5.5	–136.9	–50.7	–50.7
$\mathbf{TS_{ReN}g}$[r] + CH_3OH[g]	–114.7	–114.1	0.1	–114.1	–29.8	–29.8
$\mathbf{TS_{ReN}h}$[s] + CH_3OH[g]	–112.9	–112.3	8.2	–114.7	–28.1	–28.1
$\mathbf{TS_{rot}c}$[f] + CH_3OH[g]	–131.0	–130.0	–1.1	–129.6	–44.5	–44.5
ac-**6** + CH_3OH[g]	–133.6	–131.8	6.8	–133.8	–50.1	–50.1
sc-**6** + CH_3OH[g]	–141.4	–139.8	9.7	–142.7	–55.4	–55.4

[a]BS1 = LANL2DZ+f for the rhenium atom and 6-31G(d,p) for non-metal atoms. [b]BS2 = LANL2TZ(f) for the rhenium atom and def2-TZVP for non-metal atoms. [c]The transition state for interconverting *ac*-$\mathbf{4}^+$ and *sc*-$\mathbf{4}^+$. [d]The transition state for interconverting *ac*-$\mathbf{4}^+$ and $\mathbf{4'}^+$. [e]The transition state for interconverting *sc*-$\mathbf{5}^+$ and *ac*-$\mathbf{5}^+$. [f]The transition state for interconverting *sc*-**6** and *ac*-**6**. [g]Separately computed species. [h]The transition state for interconverting *ac*-$\mathbf{5}^+$ and *sc*-$\mathbf{5'}^+$. [i]The transition state for interconverting *sc*-$\mathbf{5}^+$ and *ac*-$\mathbf{5'}^+$. [j]The estimated maximum barrier for the conversion of *ac*-$\mathbf{5'}^+$ and $^-OCH_3$ to *ac*-$\mathbf{5'}$-OCH_3 is 8.3 kcal/mol, based upon enthalpic limits (Δ*H*(C_6H_5Cl)) provided in Table S8.[s5] [k]The estimated maximum barrier for the conversion of *sc*-$\mathbf{5'}^+$ and $^-OCH_3$ to *sc*-$\mathbf{5'}$-OCH_3 is 9.7 kcal/mol, based upon enthalpic limits (Δ*H*(C_6H_5Cl)) provided in Table S8.[s5] [l]The estimated maximum barrier for the conversion of *ac*-$\mathbf{5'}$-OCH_3 to *ac*-**6** and CH_3OH is 1.8 kcal/mol, based upon enthalpic limits (Δ*H*(C_6H_5Cl)) provided in Table S8.[s5] [m]The estimated maximum barrier for the conversion of *sc*-$\mathbf{5'}$-OCH_3 to *sc*-**6** and CH_3OH is 5.9 kcal/mol, based upon enthalpic limits (Δ*H*(C_6H_5Cl)) provided in Table S8.[s5] [n]The estimated maximum barrier for the conversion of *ac*-$\mathbf{5}^+$ and $^-OCH_3$ to *ac*-**5**-OCH_3 is 8.4 kcal/mol, based upon enthalpic limits (Δ*H*(C_6H_5Cl)) provided in Table S8.[s5] [o]The estimated maximum barrier for the conversion of *sc*-$\mathbf{5}^+$ and $^-OCH_3$ to *sc*-**5**-OCH_3 is 8.9 kcal/mol, based upon enthalpic limits (Δ*H*(C_6H_5Cl)) provided in Table S8.[s5] [p]The estimated maximum barrier for the conversion of *ac*-**5**-OCH_3 to *ac*-**7** and CH_3OH is 9.1 kcal/mol, based upon enthalpic limits (Δ*H*(C_6H_5Cl)) provided in Table S8.[s5] [q]The estimated maximum barrier for the conversion of *sc*-**5**-OCH_3 to *sc*-**7** and CH_3OH is 9.8 kcal/mol, based upon enthalpic limits (Δ*H*(C_6H_5Cl)) provided in Table S8.[s5] [r]The transition state for interconverting *ac*-**7** and *sc*-**6**. [s]The transition state for interconverting *sc*-**7** and *ac*-**6**.

Table S8. Relative solution-phase entropies (C_6H_5Cl) with solvation corrections at 1.0 atm (298.15 K) for the species in Figures S1, S8, 8, and 9 (main text).

	ωB97X-D/BS2(CPCM)//ωB97X-D/BS1[a,b]
	$\Delta H(C_6H_5Cl)$ (1.0 atm) (kcal/mol)
ac-**5′**$^+$ + $^-OCH_3$[c]	0.0
ac-**5′**-OCH_3	8.3
sc-**5′**$^+$ + $^-OCH_3$[c]	0.0
sc-**5′**-OCH_3	9.7
ac-**5′**-OCH_3	0.0
ac-**6** + CH_3OH[c]	1.8
sc-**5′**-OCH_3	0.0
sc-**6** + CH_3OH[c]	5.9
ac-**5**$^+$ + $^-OCH_3$[c]	0.0
ac-**5**-OCH_3	8.4
sc-**5**$^+$ + $^-OCH_3$[c]	0.0
sc-**5**-OCH_3	8.9
ac-**5**-OCH_3	0.0
ac-**7** + CH_3OH[c]	9.1
sc-**5**-OCH_3	0.0
sc-**7** + CH_3OH[c]	9.8

[a]BS1 = LANL2DZ+f for the rhenium atom and 6-31G(d,p) for non-metal atoms. [b]BS2 = LANL2TZ(f) for the rhenium atom and def2-TZVP for non-metal atoms. [c]Separately computed species.

Table S9. Crystallographic atom label changes for $\mathbf{4}^{+}$ $BF_4^{-}\cdot(CH_2Cl_2)_{0.5}$.

Original Label	New Label
Re1	Re1
P1	P1
N1	N2
N2	N1
N3	N3
O3	O3
B1	B1
F1	F1
F2	F2
F3	F3
F4	F4

Table S10. Crystallographic atom label changes for $\mathbf{5}^{+}$ BF_4^{-}.

Original Label	New Label	Original Label	New Label	Original Label	New Label
Re1	Re1	C21	C71	C45	C45
P1	P1	C22	C72	C46	C46
N1	N3	C23	C73	C50	C1
N10	N2	C24	C74	C51	C11
N11	N1	C25	C75	C52	C52
O1	O3	C26	C76	C53	C53
B1	B1	C31	C31	C54	C54
F1	F1	C32	C32	C55	C55
F2	F2	C33	C33	C56	C56
F3	F3	C34	C34	C61	C22
F4	F4	C35	C35	C62	C21
C11	C16	C36	C36	C63	C63
C12	C12	C41	C41	C64	C64
C13	C13	C42	C42	C65	C65
C14	C14	C43	C43	C66	C66
C15	C15	C44	C44	H10A	H1

Table S11. Crystallographic atom label changes for **6**·CH_2Cl_2.

Original Label	New Label	Original Label	New Label	Original Label	New Label
Re1	Re1	C23	C73	C46	C46
P1	P1	C24	C74	C50	C1
N1	N3	C25	C75	C51	C11
N10	N1	C26	C76	C52	C52
N11	N2	C31	C31	C53	C53
O1	O3	C32	C32	C54	C54
Cl10	Cl10	C33	C33	C55	C55
Cl11	Cl11	C34	C34	C56	C56
C11	C16	C35	C35	C61	C22
C12	C12	C36	C36	C62	C21
C13	C13	C41	C41	C63	C63
C14	C14	C42	C42	C64	C64
C15	C15	C43	C43	C65	C65
C21	C71	C44	C44	C66	C66
C22	C72	C45	C45	C100	C100

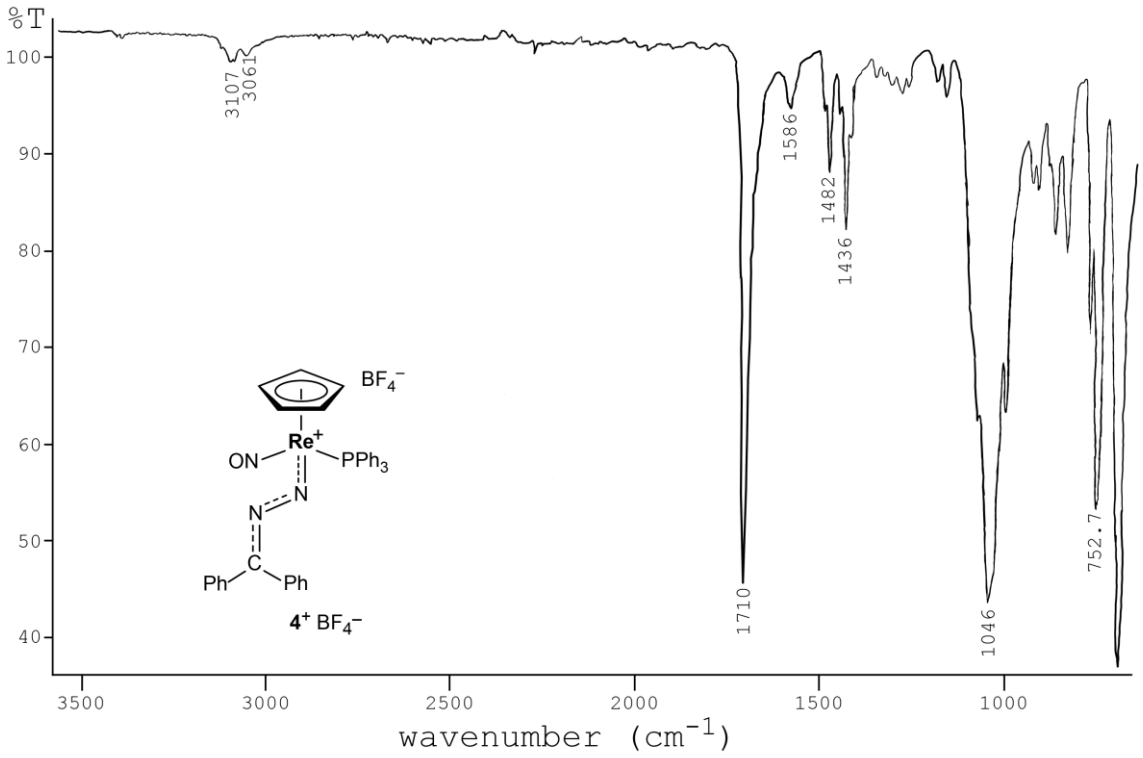

Figure S9. IR spectrum (powder film) of $\mathbf{4}^{+}$ BF_4^{-}. The original spectrum was traced over to enhance visibility.

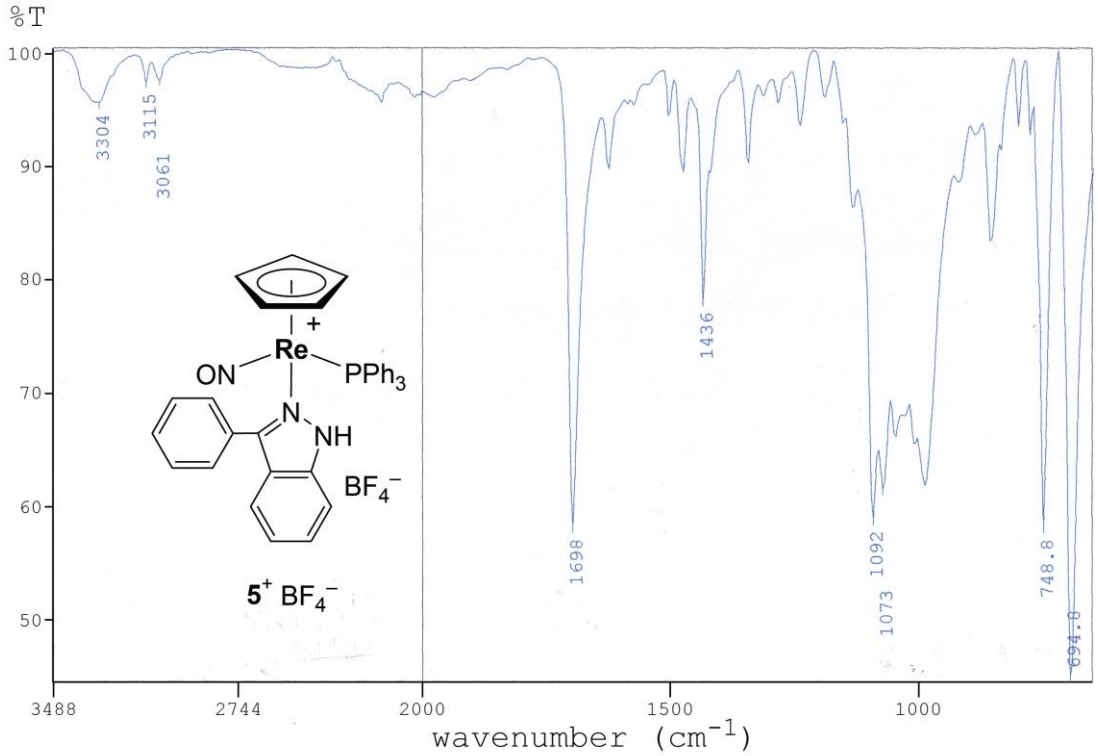

Figure S10. IR spectrum (powder film) of $\mathbf{5}^{+}$ BF_4^{-}.

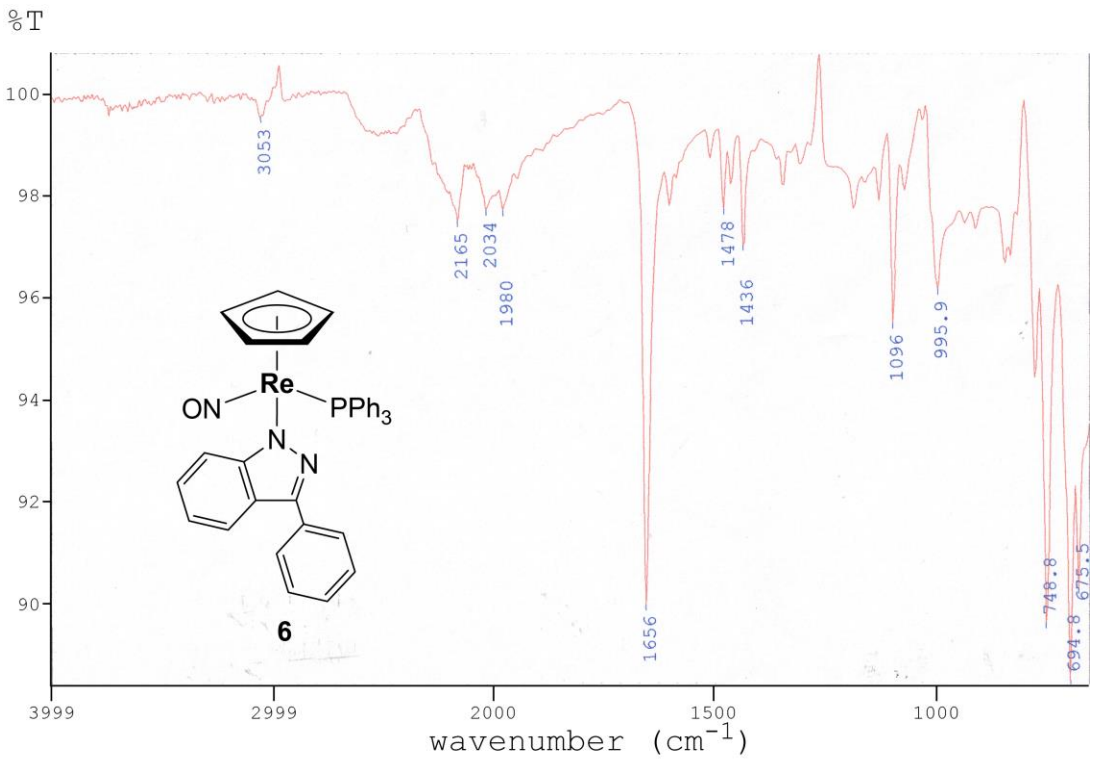

Figure S11. IR spectrum (powder film) of **6**.

Mixing $NNCPh_2$ and copper under the conditions of Scheme 1. A Schlenk flask was charged with chlorobenzene (30 mL), Et_2O (0.118 mL), copper powder (0.030 g, 0.47 mmol), and adamantane (0.057 g, 0.417 mmol; NMR standard). The suspension was cooled to –42 °C, and a solution of $NNCPh_2$ (0.486 g, 2.50 mmol) in pentanes (5.0 mL) was added via syringe. The mixture was stirred at –42 °C (1 h) and then room temperature (24 h). Aliquots were removed 1 h, 2 h, 3 h, and 25 h after $NNCPh_2$ addition. These were immediately filtered through glass wool. A portion of each filtrate (0.50 mL) and chlorobenzene-d_5 (0.25 mL) were combined. The samples were analyzed by ^{13}C NMR. No reactions were observed, and the areas of the $NNCPh_2$ signals remained constant relative to the standard.

References

(s1) Yanai, T.; Tew, D. P.; Handy, N. C. A new hybrid exchange-correlation functional using the Coulomb-attenuating method (CAM-B3LYP). *Chem. Phys. Lett*. **2004**, *393*, 51-57.

(s2) Zhao, Y.; Truhlar, D. G. The M06 suite of density functionals for main group thermochemistry, thermochemical kinetics, noncovalent interactions, excited states, and transition elements: two new functionals and systematic testing of four M06-class functionals and 12 other functionals. *Theor. Chem. Acc*. **2008**, *120*, 215-241.

(s3) (a) Perdew, J. P. Density-functional approximation for the correlation energy of the inhomogeneous electron gas. *Phys. Rev. B: Condens. Matter Mater. Phys.* **1986**, *33*, 8822-8824. (b) Becke, A. D. Density-functional exchange-energy approximation with correct asymptotic behavior. *Phys. Rev. A: At., Mol., Opt. Phys.* **1988**, *38*, 3098-3100.

(s4) Grimme, S.; Ehrlich, S.; Goerigk, L. Effect of the Damping Function in Dispersion Corrected Density Functional Theory. *J. Comput. Chem*. **2011**, *32*, 1456-1465.

(s5) Hartwig, J. F.; Cook, K. S.; Hapke, M.; Incarvito, C. D.; Fan, Y.; Webster, C. E.; Hall, M. B. Rhodium Boryl Complexes in the Catalytic, Terminal Functionalization of Alkanes. *J. Am. Chem. Soc*. **2005**, *127*, 2538-2552 (see especially Figure 10 therein).